Journal of Power Sources 498 (2021) 229885

Contents lists available at ScienceDirect

Journal of Power Sources

journal homepage: www.elsevier.com/locate/jpowsour

The origin of impedance rise in Ni-Rich positive electrodes for lithium-ion batteries

Rung-Chuan Lee [a], Joseph Franklin [a,b], Chixia Tian [a,c], Dennis Nordlund [d], Marca Doeff [a], Robert Kostecki [a,*]

[a] Energy Storage and Distributed Resources Division, Lawrence Berkeley National Laboratory, Berkeley, CA 94720, USA
[b] Electrochemical Innovation Lab, Department of Chemical Engineering, University College London, London, WC1E 7JE, UK
[c] Academy of Integrated Science, Virginia Tech, Blacksburg VA 24061, USA
[d] Stanford Synchrotron Radiation Lightsource, SLAC National Accelerator Laboratory, Menlo Park, CA 94035, United States

HIGHLIGHTS

- Degradation mechanism of Li-ion Ni-rich NMC positive electrodes was determined.
- Contact resistance in the composite electrodes mainly responsible for degradation.
- Impedance rise depends on the initial surface composition and structure of NMC.
- Surface pre-treatment of NMC supresses impedance increase during electrode cycling.

ARTICLE INFO

Keywords:
Lithium-ion battery
Ni-rich NMC
Impedance growth
Interfacial stability
Solid electrolyte interphase

ABSTRACT

The cycling performance of nickel-rich lithium nickel cobalt manganese oxide (NMC) electrodes in Li-ion batteries (LIBs) partially depends on the control of the kinetics of degradation processes that result in impedance rise. The impedance contribution from surface film formation at the NMC/electrolyte interfaces is highly dependent on the initial chemical composition and the structure of the NMC surfaces. Through comparison of film quantity and electrochemical performance of composite electrodes made of *pristine*- and *surface treated*-NMC materials, we are able to demonstrate that a simple surface treatment suppressed the subsequent film formation and reduced impedance rise of the Li/NMC half-cells during cycling. Detailed modelling of factors affecting cell impedance provide further insights to index individual interphase resistance, highlighting the underlying positive effects of the proposed surface treatment, and demonstrating the importance of homogeneous, electronically conducting matrices throughout the composite electrode.

1. Introduction

Ni-rich $LiNi_xMn_yCo_zO_2$ (NMC) ($x > y, z$) electrode materials hold great promise as next-generation high-voltage, high-capacity positive electrodes in lithium ion batteries (LIBs). However, impedance rise and capacity decay during prolonged cycling limit their practical applications [1]. Identifying, understanding, and mitigating processes responsible for the impedance increase are essential for extending cell lifetimes. Several reports have attributed impedance rise to degradation phenomena at the NMC electrode/electrolyte interface during cell operation [2]. Such processes include electrolyte oxidation [3,4], gas evolution [5], surface film formation [6–8], surface phase reconstruction [9–11], transition metal (TM) reduction and dissolution [8,12,13] primary particle cracking [14–16], side reactions at carbon additives [17], secondary NMC particles decrepitation from anisotropic structural distortion [18,19] and bulk fatigue induced by surface reconstruction [20]. Whilst it is clear that multiple degradation processes may occur in parallel or in sequence, determining which is the original and dominant cause of impedance rise in the NMC electrodes is essential for enabling Ni-rich NMC chemistry in high-energy Li-ion cells.

Degradation processes at the electrode/electrolyte interface play a key role and, as such, the electrode original surface composition and

* Corresponding author. Lawrence Berkeley National Laboratory Energy Storage and Distributed Resources Division Lawrence Berkeley National Laboratory 1 Cyclotron Rd. Berkeley, CA 94720 United States.
E-mail address: r_kostecki@lbl.gov (R. Kostecki).

https://doi.org/10.1016/j.jpowsour.2021.229885
Received 29 December 2020; Received in revised form 10 March 2021; Accepted 2 April 2021
Available online 21 April 2021

structure and their evolution during cycling have been the subject of many investigations. The surface of nickel-rich NMC particles have been shown to undergo reconstruction within the first few atomic layers of the NMC in contact with the electrolyte changing from layered-to rock salt-phases during storage or upon electrochemical cycling [9–11]. At the electrolyte side of the interface, metal-organic films have been observed on the outer layer of the electrode [21]. Electrolyte solvents, such as ethylene carbonate (EC) and diethyl carbonate (DEC), oxidize at the Li-ion high voltage positive electrode surface, producing poly-ethylene glycol [21] and β-diketonate ligands, which form coordination compounds with transition metal ions and surface films on NMC [8]. Formation of both *i)* surface reconstruction layers and *ii)* metal-organic films can lead to buildup of electronic and ionic barriers at the NMC/electrolyte interface.

A possible interdependence of these degradation processes and their impact on the overall impedance rise can be promoted or suppressed through careful materials selection, preparation and cycling regime. The NMC surface physico-chemical properties can be influenced by multiple factors; from different synthesis methods, composite electrode/cell assembling processes [22], surface treatments [23] or storage conditions [24]; seemingly similar materials can have different surface properties, which may often be difficult to detect and quantify. Differences in electrolyte additives are reported to affect the growth of surface reconstruction layers [25] and various TM oxides are also known to catalyze electrolyte oxidation [3]. Whilst there are strong hints throughout the literature, it is yet largely unknown what the influence of the electrode surface's preparation is, in terms of reactivity with the electrolyte and interfacial impedance. It is therefore important to assess the root cause and impact of such changes, in an attempt to separate out from other degradation processes that may occur in parallel. As it is demonstrated by the strict level of quality control of materials and manufacturing in commercial cells, the combinatory effect of these many seemingly small differences can significantly improve (or impede) long-term cycling performance. One relevant example of such practice for commercial cells is a pre-treatment at elevated temperatures, which occurs after cell assembly. This thermal processing constitutes part of the electrolyte wetting and formation process in LIBs, which is conventionally applied to develop a stable solid electrolyte interphase (SEI) on the anode. The exact details of electrolyte wetting and formation processes for commercial cells (the temperatures and duration used) are not well documented in the literature and the effects of the formation process on the positive electrode are not well understood.

In this study, nickel-rich NMC powder was pre-treated via exposure to the electrolyte at 60 °C to understand what effect this process has on *i)* the electrode surface and *ii)* the electrode electrochemical performance in a battery cell. A far less aggressive processing procedure, has been shown in other work to result in modest surface reconstruction to rock salt [9]. Lin et al. [9] found that soaking NMC powders in electrolyte at room temperature led to shallow (a few nm) changes in particle surface structure, specifically a surface reconstruction. The treatment used in the presented work is at higher temperature (60 °C vs. room temperature) and for longer duration (240 vs. 30 h) compared to the work in the previous study by Lin et al. The more aggressive treatment presented here simulates the elevated temperatures in the electrolyte wetting and formation procedure for commercial LIB cells; allowing us to investigate how such treatment changes the NMC electrode/electrolyte interface and its influence on the cell degradation. We demonstrate that the surface pre-treatment of NMC in the electrolyte at elevated temperatures has a positive effect on the subsequent electrode impedance and long-term electrochemical performance.

2. Experimental

2.1. Surface pretreatment of NMC particles and preparation of composite electrodes

The following electrolyte-exposure process was used to modify NMC particles: $LiNi_{0.5}Mn_{0.3}Co_{0.2}O_2$ (NMC-532, Umicore TX10) particles were soaked in the 1 M $LiPF_6$ in ethylene carbonate/diethyl carbonate (1:2 vol) electrolyte with 1:1 wt ratio at 60 °C in an Ar atmosphere for 10 days. For each gram of NMC powder 10 ml of electrolyte was used in the pretreatment process. Then, the NMC particles were washed with DEC in an ultrasonic bath, and finally dried in vacuum at room temperature. Both pristine NMC and pre-treated NMC powders were used as active materials to prepare composite electrodes for investigation. The composite electrodes consisted of 92.8 wt% NMC active material, 3.2 wt% carbon black (Acetylene Black), and 4 wt% PVdF (Kureha). A slurry of these powders in *N*-Methyl-2-pyrrolidone solvent was doctor-bladed onto Al foil and dried in Ar-filled glove box at 20 °C, 1 atm for 12 h. The electrodes were subsequently roll pressed at 100 °C to 50% of their original thickness and punched out into 12 mm diameter foils. Typical electrodes were ~20 μm thick and contained ~5 mg cm^{-2} active material. Prepared electrodes were dried in Ar-filled glove box antechamber vacuum oven at 120 °C, 0.2 Torr for 12 h.

2.2. Coin cell assembly and testing

2325 coin cells were assembled with Li-foil anodes and Celgard® 2300 separators wetted with 1 M $LiPF_6$ in ethylene carbonate/diethyl carbonate = 1:2 electrolyte and NMC composite electrodes. The electrochemical measurements were performed using a VMP3 potentiostat (model 273 A) with frequency response analyzer (model FRD100).

Each cell underwent two preliminary formation charge discharge cycles at constant current of 20 mA g^{-1} (~0.1 C-rate) between 3.0 and 4.2 V followed by cycle-life testing carried at 100 mA g^{-1} (~0.5 C-rate) at 25 °C. A total of 7 cells were prepared: 2 pairs of cells with pristine and pre-treated NMC were cycled between 2 and 4.7 V, and one pair of cells with pristine and pre-treated NMC were cycled between 2 and 4.5 V, and 1 cell with pristine NMC which was held at 60 °C for 12 h after assembly. The impedance of each cell was measured at 4 V at selected cycles over a frequency range of 0.1 Hz–100 kHz. Rate performance of the electrode was tested in the current density range 17–2000 mA g^{-1}. All tests and measurements were carried out at ambient temperature.

2.3. Chemical and physical characterization of the NMC electrodes

For characterization of the cycled electrodes, the cell was fully discharged at 0.1 C-rate to 2.0 V, and disassembled in an Ar glovebox. Then, the NMC electrodes were washed in dimethyl carbonate (DEC) for 3 h and dried in vacuum overnight prior to evaluation. The surface morphology of the NMC particles was characterized by scanning electron microscopy (SEM, JEOL, JSM-7500F). Fourier Transform Infrared Spectroscopy (FTIR) measurements were performed on a Shimadzu IRTracer-100 system. To prepare the samples for FTIR, powder samples or composite samples removed from cycled electrodes were mixed with KBr and pressed into pellets. FTIR spectra were recorded in an N_2-filled environmental chamber and acquired in transmission mode. Raman measurements were performed on a Raman microscope system (Horiba Jobin Yvon USA, Inc.) with an Ar-ion laser (Lexel Laser TM) tuned at 488 nm. Spectra were recorded with an 80x microscope objective (Olympus America Inc.) with the laser power ≤1 mW and a laser spot size at the sample of ~2 μm in diameter. X-ray diffraction (XRD) on powder samples was performed on a Bruker D2 Phase diffractometer using CuKα radiation.

XAS measurements were performed on beamline 8–2 at Stanford Synchrotron Radiation Lightsource (SSRL) using a ring current of 500 mA and a 1000 lines mm^{-1} spherical grating monochromator with 40

μm entrance and exit slits, providing ~2*10^{10} ph s^{-1} at 0.2 eV resolution in a 0.1*0.1 mm^2 beam spot. During the measurements, all electrode samples were attached to an aluminum sample holder using conductive carbon tape. Data were acquired under ultrahigh vacuum (10^{-9} Torr) in a single load at room temperature using TEY and sample drain current was collected for TEY. Contributions from visible light were carefully minimized before the acquisition, and all spectra were normalized by the current from freshly evaporated gold on a fine grid positioned upstream of the main chamber. The residual organic content of cycled NMC electrodes after washing were analyzed using a thermogravimetric analyzer (TGA, TA Instruments, SDT-Q600) with temperature ramping from room temperature to 600 °C at the heating rate of 5 °C per min.

3. Results and discussion

3.1. Electrochemical behavior of pristine and pretreated NMC composite electrodes

The electrochemical performance of the composite electrodes prepared from pristine NMC and the pre-treated NMC 532 powders was evaluated at *ca.* 0.5 C-rate between 2 - 4.7 V and 2–4.5 V. Fig. 1 shows the charge-discharge voltage profiles for the 2nd and 100th cycles. At the beginning of the long-term cycling both electrodes display a very similar behavior, suggesting that the pretreatment has no significant effect on the initial capacity and impedance of the NMC electrode. Similarly, in the 2–4.7 V range, pristine and pre-treated NMC electrodes show no major difference in the 1st cycle coulombic efficiency, which was 88.9% and 89.5%, respectively. After 100 cycles between 2 and 4.7 V, the pristine and pre-treated NMC electrodes showed 23.2% and 20.4% capacity loss, respectively. Moreover, the pristine NMC electrode displayed a noticeable higher ohmic polarization than the pretreated NMC electrode. The pre-treated NMC also outperformed the untreated NMC by a larger margin upon cycling between 2 and 4.5 V with better capacity retention and less ohmic polarization after 100 cycles. This is also consistent with the NMC/Li half-cell rate performance evaluation data (Fig. 2), which show more capacity retention in 2–4.7 V range and lower ohmic polarization at current densities higher than 200 mA/g; i.e., ca. 1C rate. These results were fully reproducible for duplicate cells tested under the same conditions.

Fig. 3 shows the Nyquist plots of the complex impedance of the NMC/Li half-cells at OCV after cutoff at 4 V during the charging process for the 2nd and 100th cycles between (a) 2–4.7 V and (b) 2–4.5 V. The impedance plots of the fresh electrodes (2nd cycle) show one flattened

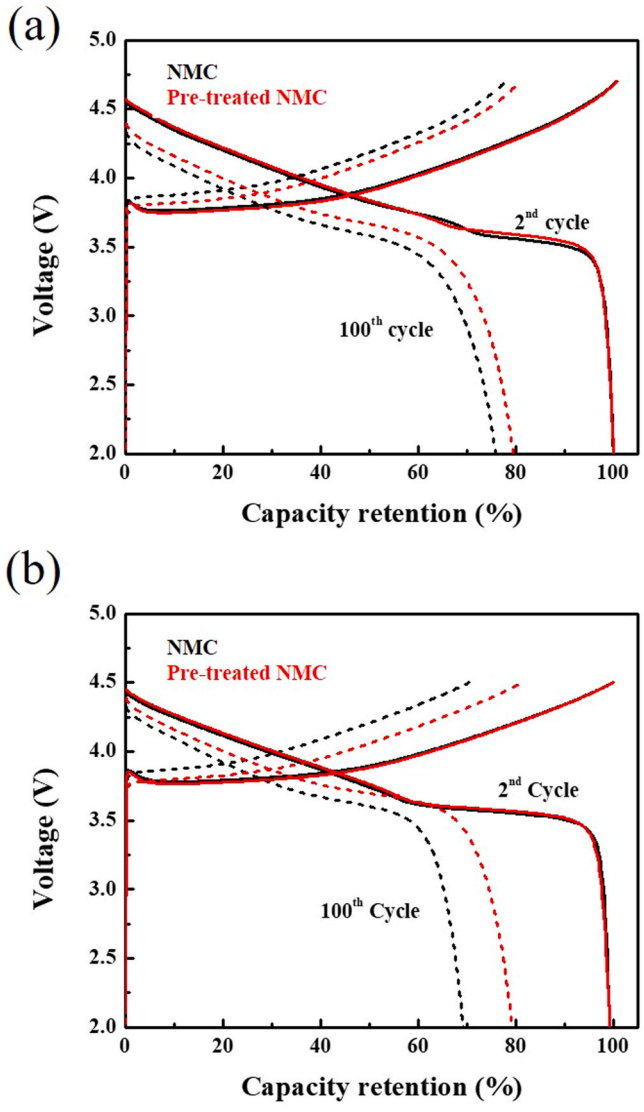

Fig. 1. Charge-discharge curves of half-cells containing pristine and pre-treated NMC electrodes for the 2nd (solid line) and 100th (dashed line) cycle during galvanostatic cycling between 2 – 4.7 V (a) and 2 – 4.5 V (b) at 100 mA g^{-1} (~0.5 C-rate).

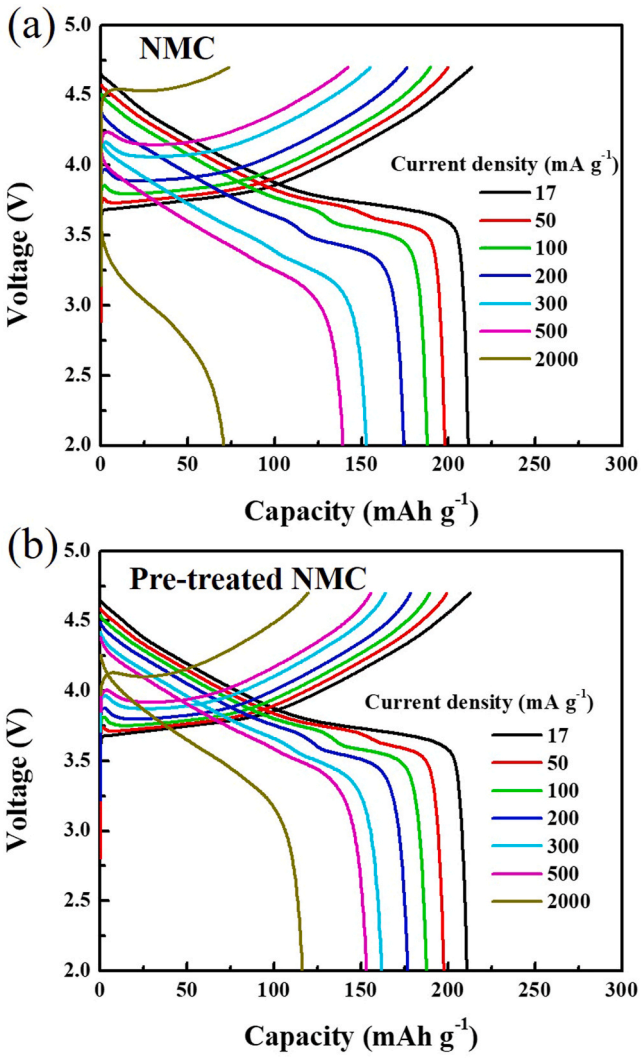

Fig. 2. Charge-discharge curves of half-cells containing pristine (a) and pre-treated NMC electrodes (b) for galvanostatic cycling between 2 – 4.7 V at different current densities.

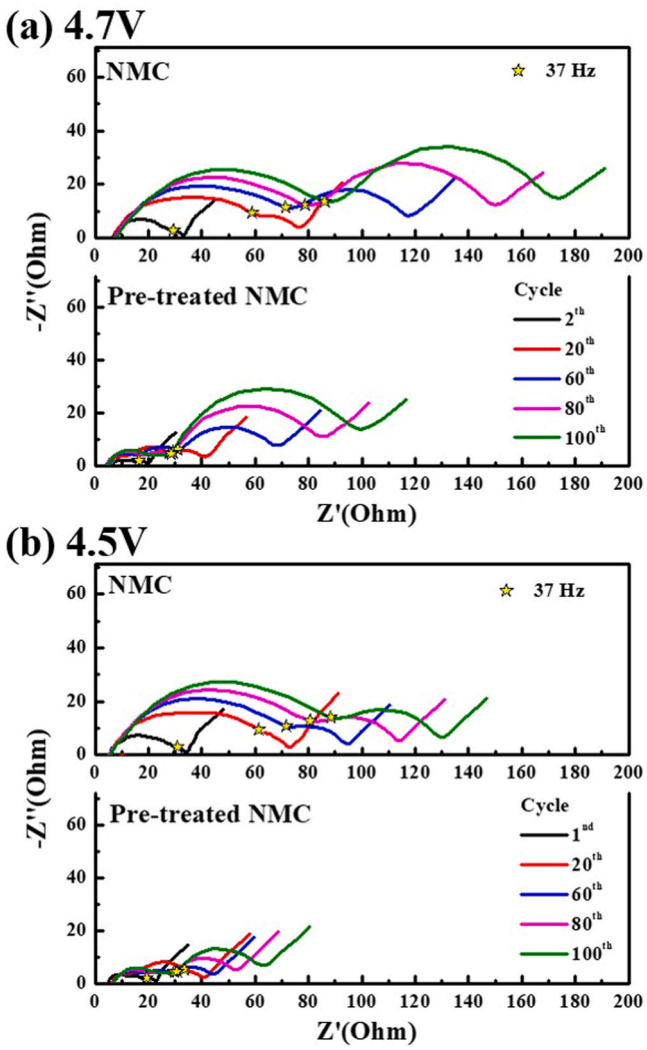

Fig. 3. Nyquist plots of the complex impedance of half-cells containing pristine and pre-treated NMC electrodes at 4 V during galvanostatic cycling between (a) 2 – 4.7 V and (b) 2 - 4.5 V at 100 mA g^{-1} (~0.5 C-rate).

semicircle followed by a low frequency Warburg component that represents diffusion though a semi-infinite medium. Contrary to the cycling data at 0.5 C-rate, the overall cell impedance of the fresh pretreated NMC electrode was ca. 30% lower than the fresh pristine NMC cell. As the cycling continued, the impedance spectra of both NMC electrodes showed impedance rise and a rapid emergence of the second low-frequency semicircle. The yellow stars mark 37 Hz, which roughly separates the impedance spectra between two low- and high-frequency semicircles. The overall cell impedance of the cells with pristine NMC electrode after 100 cycles was almost twice that of the cells with the pretreated NMC electrode.

Interestingly, the impedance rise of the cell with pretreated NMC seems to occur mainly in the lower frequency semicircle area whereas the cell impedance rise for the pristine NMC electrode happened across the whole frequency range no matter whether the upper voltage limit was 4.5 V or 4.7 V. The pristine NMC electrode cells show a fast growth of the high-frequency semicircle from 20 to 55 Ω in the first 20 cycles and then the impedance increases at a slower rate for the following cycles. The high-frequency semicircle of the cells with the pre-treated NMC electrode increased from 10 to 30 Ω in 20 cycles, after which it remained almost constant during subsequent cycles. The impedance growth in the low-frequency range (~37 Hz–~0.1 Hz) is linear with the number of cycles for both cells, but the slope of impedance rise doubled when cells were charged to 4.7 V vs. 4.5 V, indicating the acceleration of electrode degradation processes at high potentials. Nevertheless, the cells equipped with pre-treated NMC electrode consistently showed slower impedance growth in this frequency range than the pristine NMC cells.

3.2. *Characterization of pristine and pre-treated NMC before and after cycling*

Advanced surface and bulk analysis techniques were employed to identify possible origins of the observed differences in electrochemical performance of pristine and pre-treated NMC electrodes. No clear differences between the pristine and pretreated NMC powders after washing in DEC were observed using SEM, IR, Raman, and XRD measurements (see Fig. S1 and Fig. S2 in supplementary materials), i.e., no appreciable differences in NMC surface morphology, bulk chemical composition, and structure were observed within the detection limits of the respective techniques. However, the pretreated NMC powder before washing in DEC shows a thick layer of electrolyte decomposition products, which is strongly fluorescent and consist of a mixture of organic and inorganic compounds. This suggests that the electrolyte reacted with NMC and possibly affected the surface properties of the NMC particles.

The FTIR spectra of the fresh and cycled electrodes are compared in Fig. 4a. Most peaks in the fresh electrode can be indexed to the PVdF binder (the vibration modes of NMC are located at lower frequencies and are not shown in the spectra). After cycling, new peaks at 1730 and 1610 cm^{-1} emerge, which can be indexed to the asymmetric vibration of –C═O from organic carbonate species [6,26]. These peak positions are different from the signature at 1805 and 1770 cm^{-1} of the EC residue [27] and are presumed to result from electrolyte decomposition products with β-diketone ligands [8]. The Raman spectra of the cycled electrodes (Fig. 4b) exhibit strong fluorescent backgrounds, which is related to the presence of TM-organic coordination compounds from the electrolyte oxidation and TM dissolution reactions at NMC particle surfaces [8]. Interestingly, the cycled pre-treated NMC electrode shows a significantly (3X) lower fluorescence intensity than the cycled pristine NMC electrode, indicating lower amount of metal-organic coordination compounds at the surface of the electrode.

To further quantify the amount of organic film formation during cycling, the TGA profiles of the as-prepared uncycled and cycled NMC composite electrodes are compared in Fig. 4c. The weight loss of pristine NMC (unwashed), pre-treated NMC (unwashed), cycled & washed pristine NMC and cycled & washed pre-treated NMC electrodes after heating to 650 °C are 6.4%, 6.4%, 11.4% and 8.0%, respectively. Given that the temperature was limited to 650 °C, the observed weight loss difference between fresh and cycled electrodes is assumed to come from organic components in the electrode with the inorganic components remaining largely unaffected. It is anticipated that much of the loss from fresh pristine and pre-treated NMC electrodes is from the PVdF binder (4%) and possible organic residues from the electrode manufacturing process (*e.g.* NMP) adsorbed on the conductive carbon additive. The additional weight loss from the cycled samples would therefore indicate the removal of additional organic compounds formed during cycling [28], which were not removed with washing, and including any solvent residues trapped inside the pores of the composite electrode, carbon additive, and organic film on the electrode surface. From these results, we postulate that the pre-treated NMC material produces less organic side reaction products during cycling, which is consistent with reduced catalytic activity of the treated surface compared to the pristine NMC material. This surface film may contribute to the growth of electronic- or ionic-resistance during the electrode and cell operation.

In order to probe the NMC structure and chemical composition at shallow depths (2–5 nm) from the particle surface, X-ray absorption spectroscopy in total electron yield mode (XAS-TEY) was used. Fig. 5 shows XAS spectra at the Ni, Co and Mn L-edges for the pristine and pre-

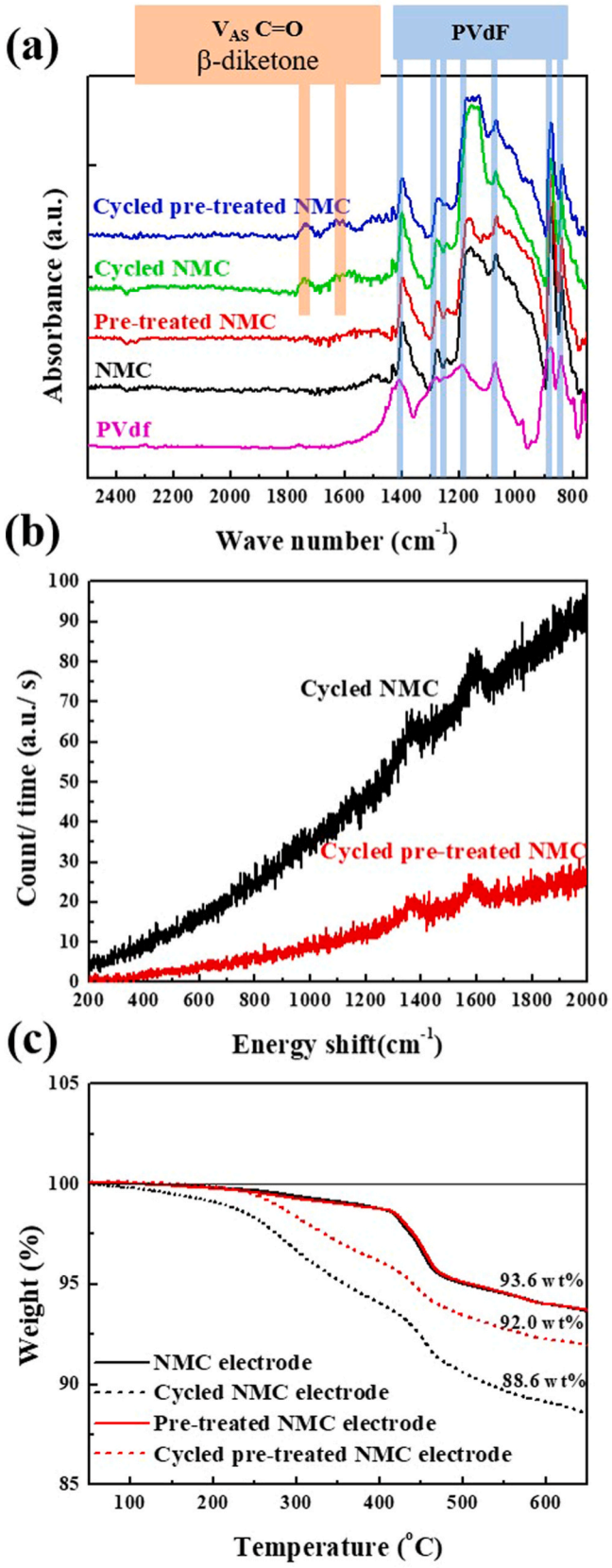

Fig. 4. (a) FTIR, (b) Raman spectra and (b) TGA profiles of the pristine NMC and pre-treated NMC electrodes before and after 100 cycles between 2 - 4.7 V at 0.5 C-rate.

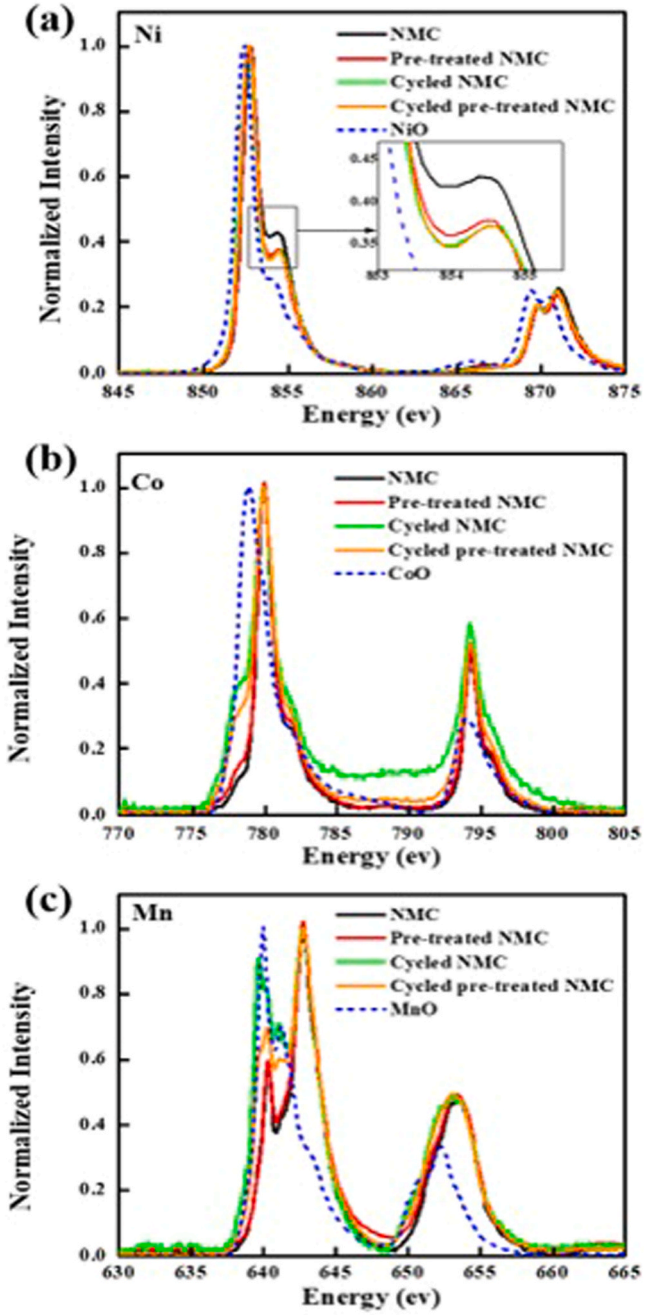

Fig. 5. X-ray absorption spectroscopy in TEY mode of fresh and 2-4.7 V cycled pristine and pre-treated NMC electrodes at the Ni L-edge (a), Co L-edge (b), and Mn L-edge (c).

treated electrodes before and after 100 cycles in 2–4.7 V. In the case of Ni, the ratio of the high energy L_3 peak to the low energy one in the L_3 double peak centered near 853 eV contains information about the average oxidation state near the surface (TEY mode probes approximately 5 nm into the surface). A lower L_{3high}/L_{3low} ratio is indicative of a lower average oxidation state for Ni, as is observed for the pre-treated NMC compared to the pristine sample before cycling. Likewise, the small shoulder at lower energies observed in the Co L-edge spectrum of the treated sample also suggests a slightly lower average oxidation state for this metal at the surface of the pre-treated sample. There is also similar evidence for slight reduction of Mn. In other words, the XAS-TEY spectra indicate that there may be a partial reduction of TM on NMC surfaces after the exposure to electrolyte at elevated temperatures,

although the effect is very modest. Whilst this reduction is consistent with surface reconstruction to rock salt [9,11,29], it is less pronounced than observed by Lin et al., where they observed extensive reduction of Ni after extensive cycling [9].

The XAS spectra of cycled NMC electrodes (Fig. 5) clearly show that the extent of Ni reduction at the surface of NMC after 100 cycles is almost the same. Taking into account the amount of partial surface TM reduction that occurred during the pretreatment of NMC in the electrolyte, we observe much less Co and Mn reduction after 100 cycles for the pre-treated NMC electrodes compared to the pristine ones, suggesting less surface reconstruction and/or formation of reduced metal-organic species at the surface during cycling. This suggests that the rate of surface reduction and associated processes (*e.g.* metal dissolution, surface film formation) during cycling is strongly dependent on the initial state of the surface. We observe that the surface treatment and creation of the reduced TM layer on NMC surface appears to slow down the subsequent TM reduction and electrolyte oxidation processes during cycling, which may play a key role in extending battery lifetime. The observed positive effects on degradation rate, result from a relatively minor observable difference in the NMC surface structure that is possibly coupled with other degradation processes at the electrode-electrolyte interface during cycling.

3.3. Impedance analysis and mechanism of NMC electrode degradation

To assign the impedance individual contributions of the NMC electrode or lithium anode, a symmetrical cell containing two cycled NMC electrodes was analyzed. Two Li/NMC half-cells (A and B) were galvanostatically cycled at 100 mA g^{-1} (~0.5 C-rate) between 2 and 4.7 V for 100 cycles and cutoff at 4 V during charge which located state-of-charge at a.u. 60%, the impedance measured, and then the cells were disassembled. Then a symmetrical cell with two cycled NMC electrodes was assembled, filled with the fresh electrolyte and the cell impedance was measured. The Nyquist plot of the cell impedance (Fig. 6) shows that the diameters of the two semi-circles from the symmetric cell are almost twice that of the individual half-cells, demonstrating that both the impedance from high and middle frequency semi-circles mostly arise from the NMC electrode.

To explain how the surface treatment helps reduce impedance rise via suppressing transition metal reduction and the associated surface film formation during prolonged cycling, the following sections analyze and discuss causes of impedance in more detail. To correlate the observed impedance contributions across different frequency ranges with interfacial processes in the composite NMC electrode, an impedance data simulation was utilized. By combining composite electrode distributed impedance models already reported in the literature [30–32], a simplified four-particle model was used to simulate the impedance behavior of the NMC composite electrode. The resistances considered and their abbreviations are given in Table 1. In this model depicted in Fig. 7a, four NMC particles are aligned in one stack perpendicular to the current collector and direct contact with the conductive carbon matrix aligned in the same direction. Each NMC particle has a single point of contact with the carbon matrix, which forms an *electron bridge* between the current collector and each NMC particle. NMC particle cracking is known to be one of the major issues in degradation, with one of the major effects being broken electronic conduction pathways as well as exposure of new surfaces to electrolyte [14–16]. Here, particle cracking is simulated by depicting each single particle as divided into three equal reaction parts having a crack resistance (R_{cr}), connected in series.

Based on these principles and assumptions, the model equivalent circuit was constructed with the various interface impedances and capacitance elements as shown in Fig. 7b. Each element is physically described and is given a set control value, listed in Table 1. The Warburg impedance element is absent in this model under assumption that this system under the current experimental conditions is not ion diffusion limited. The simulation results are shown in Fig. 7c, demonstrating two arcs with diameters of a similar magnitude and turning point at ~37 Hz (marked by yellow stars), separating high- and low-frequency semi-circles, as observed in the Nyquist plots of the experimental data

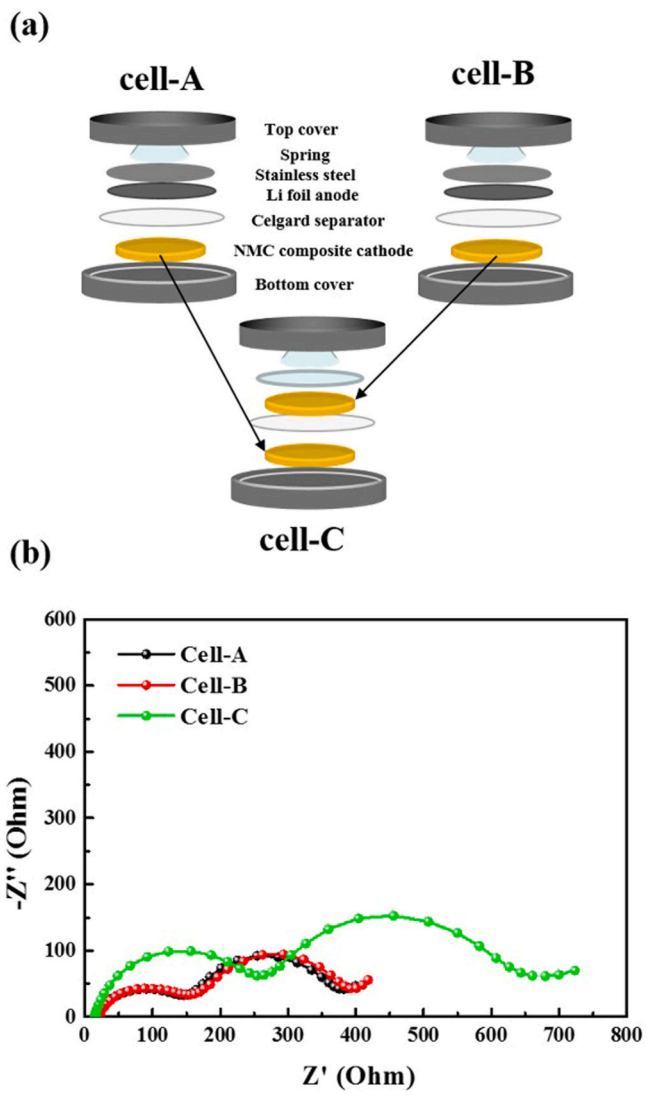

Fig. 6. Schematic diagram (a) and impedance Nyquist plot of the Li/NMC half cells (A and B), and symmetrical NMC/NMC cell (C) with NMC composite electrodes (b).

Table 1
The description and control values of elements for Nyquist plot simulation.

Element	Description	Value	Unit
RI	Electronic resistance of circuit connected out of the cell	0	Ω
Ri	Electrolyte resistance	5	Ω
RAl	Aluminum surface resistance	10	Ω
Rc	Electronic contact resistance between carbon and NMC	10	Ω
Rf	Ionic resistance of the film between NMC and electrolyte	0	Ω
Re1	Electronic resistance of carbon between Al and 1st layer of NMC	10	Ω
Re2	Electronic resistance of the carbon chain between two nearby NMCs	50	Ω
Rct	Charge transfer resistance	300	Ω
CAl	Interface capacitance on Aluminum surface	10^{-6}	F
Cr	Interface capacitance on NMC surface	$3.33*10^{-4}$	F

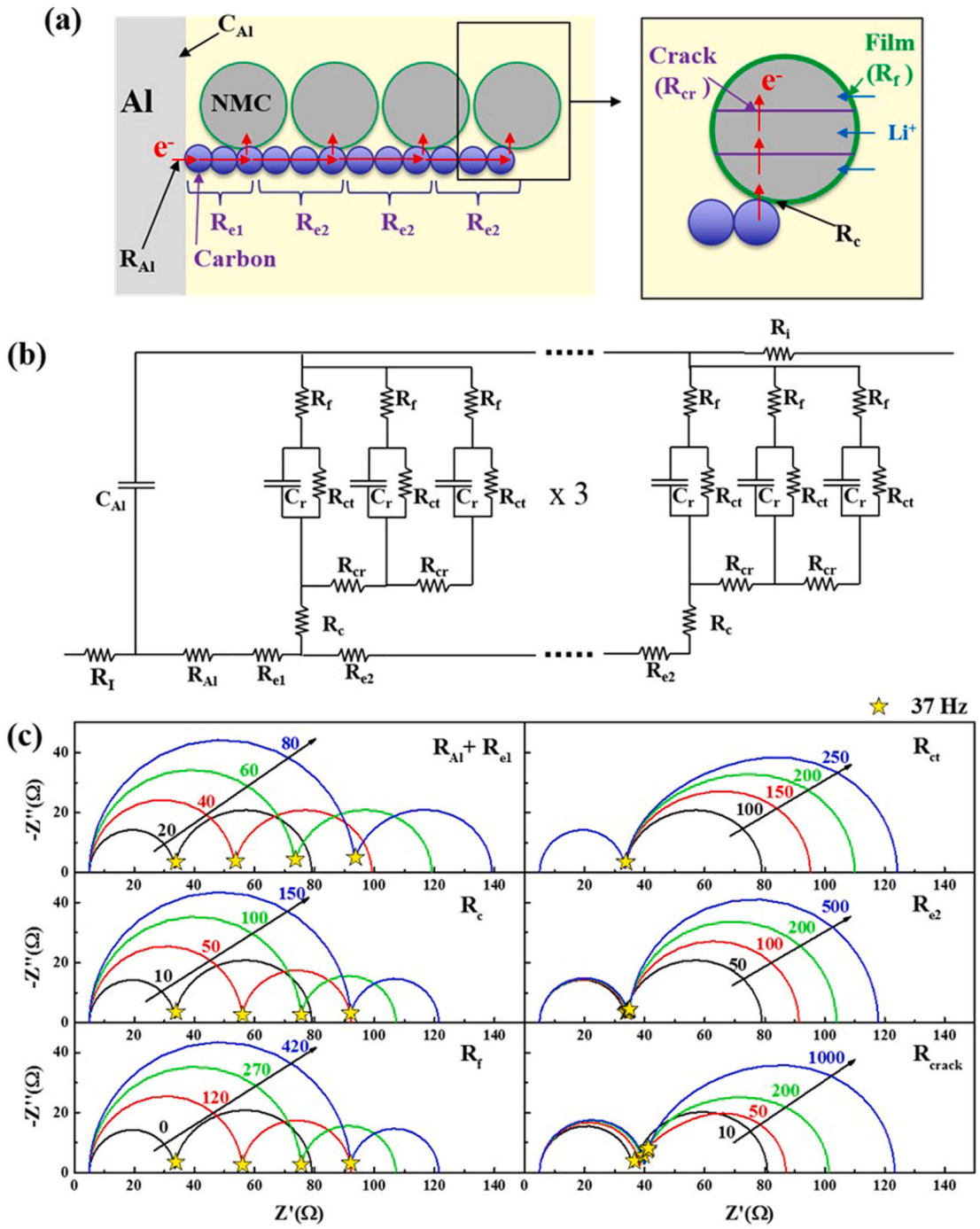

Fig. 7. (a) Schematic diagram of resistances in NMC electrodes using a four-particle model system and (b) equivalent circuit model of the NMC composite electrode. (c) Simulated Nyquist plots using different resistances.

described in this work. By systematically varying the values of each impedance individually, we were able to deduce the individual contributions to the electrode overall impedance and derive the mechanism of these complex inter-related degradation processes and their resulting impact on the electrode performance.

As the R_{Al} and R_{e1} are simply connected in series, changes in either result in equal overall effects on the Nyquist plot. When any of $R_{Al} + R_{e1}$, R_c or R_f increase, the high frequency arc would be subsequently enlarged, however there is little or no change observed for the low-frequency arc, shown in Fig. 7c. This result is consistent with a similar explanation in the literature, showing that the high frequency arc impedance rise can be attributed to the rise of either interfacial resistance with aluminum [30,33], the carbon matrix-NMC contact resistance [34] or the lithium ion diffusion resistance affected by the surface film [26].

Comparing this simulation with the EIS results shown in Fig. 3, the source of this impedance difference can be narrowed down to either R_c (NMC-carbon contact resistance) or R_f in this case, since the major observable difference between the NMC and pre-treated NMC cycled electrodes is the reduced surface and the increased formation of organic products after cycling for the former. It implies that thicker metal-organic film formation on pristine NMC surfaces will result in higher R_c and R_f resistances, compared the thinner film at the surfaces of the pre-treated NMC, as shown by the characterization results. Thus, the

pre-treatment of NMC is inferred to suppress the increase of contact resistance between NMC and carbon matrix or film ionic resistance rise by impeding organic surface film formation at NMC surface during cycling.

The low-frequency impedance rise is mainly affected by increasing the charge transfer resistance (R_{ct}), carbon chain resistance (R_{e2}), and particles crack resistance (R_{cr}). Both carbon chain resistance (R_{e2}) [35–37] and crack resistance (R_{cr}) [14,15,18,38], can be identified as the sources of inhomogeneity in electron conductivity. From the simulation results of Abarbanel et al. and Petibon et al., all the resistance of the low-frequency impedance semi-circle is attributable to charge transfer resistance [32,39]. However, our simulation demonstrates that the mid-frequency impedance can also be attributed to the electronic resistance of the carbon black network or particles cracking. We infer that a higher cut-off voltage might enhance the degree of carbon additive degradation and electrolyte decomposition on carbon [17] and particles cracking [13,17,37], resulting in a fractal structure of the cycled NMC electrode, causing faster impedance rise.

To demonstrate if similar improvements in electrochemical performance could be imparted by NMC aging at elevated temperature as part of the cell formation process protocol, a half-cell with pristine NMC electrode and Li anode was stored at 60 °C for 7 days after assembling, and then cycled at room temperature. Fig. 8 shows that impedance behavior of the treated cell was almost identical to those cells made with pre-treated NMC electrode. We therefore surmise that this treatment, whilst having a positive effect on the electrode and electrode/electrolyte interface within the studied conditions, does not appear to have any significant detrimental effect on other parts of the half-cell *e.g.* on the electrolyte. Therefore, we postulate that this simple pre-treatment of the NMC electrode material as well as full Li-ion cells can provide an efficient, non-expensive method to improve the cycling performance of NMC-based Li-ion cells for practical applications.

4. Conclusions

We demonstrated that a simple pre-treatment of NMC powder in 1 M $LiPF_6$ EC:DEC (1:2 vol) electrolyte at 60 °C helps improve long-term electrochemical performance of NMC composite electrodes. Through an electrochemical evaluation, chemical analysis, and impedance data modelling of surface pre-treated and pristine NMC electrodes, we clarified how organic surface layer formation that is coupled with partial TM reduction at NMC surface during cycling contributes to NMC-carbon electronic contact resistance and electrode impedance rise in the NMC composite electrode. Because the pre-treatment of NMC materials leads to partial reduction of TM at the surface, pre-treated NMC experiences less subsequent surface reduction and associated organic film formation, and less impedance rise after electrochemical cycling than the pristine NMC material. Using a comprehensive and systematic simulation of the impedance profiles, we identified the NMC surface film resistance and inhomogeneous electronic conductivity of the NMC electrodes as the main causes of capacity fading. We show that seemingly small changes to the surfaces of these commercially important Li-ion positive electrode materials can change the kinetics of interfacial processes and reduce degradation, prolonging the cycle life of battery materials. We demonstrated how this knowledge can be directly and conveniently applied after cell assembly for improved lifetime and performance. The findings expose the importance of the development of the positive electrode interface during pre-treatment and formation protocol in industry in terms of long-term stability, rather than only the anode side.

CRediT authorship contribution statement

Rung-Chuan Lee: Conceptualization, Investigation, Writing – review & editingwriting-reviewing and editing. **Joseph Franklin:** Conceptualization, Investigation, Writing – review & editing. **Chixia Tian:** Investigation. **Dennis Nordlund:** Investigation. **Marca Doeff:** Investigation. **Robert Kostecki:** Oversight and leadership responsibility for the research activity, Writing – review & editing.

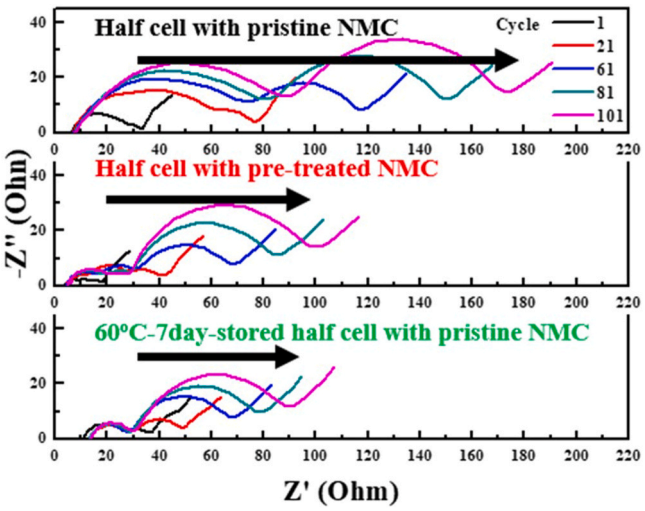

Fig. 8. Impedance spectra of half-cells with pristine NMC, pre-treated NMC cathodes, and half-cell with pristine NMC that was stored at 60 °C for 7 days and then galvanostatically cycled at 100 mA g^{-1} (~0.5 C-rate) between 2 - 4.7 V. The black arrows represent the increasing AC impedance at 0.1 Hz of each cell from the 1st cycle to 101st cycle.

Declaration of competing interest

The authors declare that they have no known competing financial interests or personal relationships that could have appeared to influence the work reported in this paper.

Acknowledgments

This work was supported by the Assistant Secretary for Energy Efficiency and Renewable Energy, Office of Vehicle Technologies, U.S. Department of Energy, under Contract DEAC02-05CH11231. Use of the Stanford Synchrotron Radiation Lightsource, SLAC National Accelerator Laboratory, is supported by the U.S. Department of Energy, Office of Science, Office of Basic Energy Sciences under Contract No. DE-AC02-76SF00515. The authors gratefully acknowledge Dr. Vincent S. Battaglia and Dr. Yanbao Fu (LBNL) for supplying electrode materials, Dr. Ethan Crumlin, Dr. Wanli Yang (ALS/LBNL) for fruitful discussions and Dr. Liang Zhang and Dr. Jinghua Guo (ALS/LBNL) for refinement of XAS data and database support. JBF acknowledges support from the European Union Horizon 2020 under the Marie Sklodowska-Curie grant agreement No. 705339 and is grateful for support from the Science and Technology Facilities Council Early Career award, ST/K00171X/1.

Appendix A. Supplementary data

Supplementary data to this article can be found online at https://doi.org/10.1016/j.jpowsour.2021.229885.

References

[1] H.J. Noh, S. Youn, C.S. Yoon, Y.K. Sun, J. Power Sources 233 (2013) 121–130.
[2] T. Osaka, D. Mukoyama, H. Nara, J. Electrochem. Soc. 162 (2015) A2529–A2537.
[3] Y.S. Duh, Y.L. Chen, C.S. Kao, J. Therm. Anal. Calorim. 127 (2017) 995–1007.
[4] J. Xia, R. Petibon, A. Xiao, W.M. Lamanna, J.R. Dahn, J. Power Sources 330 (2016) 175–185.
[5] D.J. Xiong, L.D. Ellis, K.J. Nelson, T. Hynes, R. Petibon, J.R. Dahn, J. Electrochem. Soc. 163 (2016) A3069–A3077.
[6] D.T. Nguyen, J. Kang, K.M. Nam, Y. Paik, S.W. Song, J. Power Sources 303 (2016) 150–158.

[7] L. Madec, R. Petibon, K. Tasaki, J. Xia, J.P. Sun, I.G. Hill, J.R. Dahn, Phys. Chem. Chem. Phys. 17 (2015) 27062–27076.
[8] A. Jarry, S. Gottis, Y.S. Yu, J. Roque-Rosell, C. Kim, J. Cabana, J. Kerr, R. Kostecki, J. Am. Chem. Soc. 137 (2015) 3533–3539.
[9] F. Lin, I.M. Markus, D. Nordlund, T.C. Weng, M.D. Asta, H.L.L. Xin, M.M. Doeff, Nat. Commun. 5 (2014).
[10] S.K. Jung, H. Gwon, J. Hong, K.Y. Park, D.H. Seo, H. Kim, J. Hyun, W. Yang, K. Kang, Adv. Energy Mater. 4 (2014).
[11] F. Lin, D. Nordlund, I.M. Markus, T.C. Weng, H.L. Xin, M.M. Doeff, Energy Environ. Sci. 7 (2014) 3077–3085.
[12] L. Mu, X. Feng, R. Kou, Y. Zhang, H. Guo, C. Tian, C.-J. Sun, X.-W. Du, D. Nordlund, H.L. Xin, F. Lin, Adv. Energy Mater. 8 (2018) 1801975.
[13] H.H. Zheng, Q.N. Sun, G. Liu, X.Y. Song, V.S. Battaglia, J. Power Sources 207 (2012) 134–140.
[14] C.H. Shen, Q. Wang, H.J. Chen, C.G. Shi, H.Y. Zhang, L. Huang, J.T. Li, S.G. Sun, Acs Appl. Mater. Inter. 8 (2016) 35323–35335.
[15] P.F. Yan, J.M. Zheng, M. Gu, J. Xiao, J.G. Zhang, C.M. Wang, Nat. Commun. 8 (2017).
[16] H. Kim, M.G. Kim, H.Y. Jeong, H. Nam, J. Cho, Nano Lett. 15 (2015) 2111–2119.
[17] J. Syzdek, M. Marcinek, R. Kostecki, J. Power Sources 245 (2014) 739–744.
[18] J.M. Lim, T. Hwang, D. Kim, M.S. Park, K. Cho, M. Cho, Sci. Rep-Uk 7 (2017).
[19] J.A. Gilbert, I.A. Shkrob, D.P. Abraham, J. Electrochem. Soc. 164 (2017) A389–A399.
[20] C. Xu, K. Märker, J. Lee, A. Mahadevegowda, P.J. Reeves, S.J. Day, M.F. Groh, S. P. Emge, C. Ducati, B. Layla Mehdi, C.C. Tang, C.P. Grey, Nat. Mater. (2020).
[21] Y.M. Liu, B.G. Nicolau, J.L. Esbenshade, A.A. Gewirth, Anal. Chem. 88 (2016) 7171–7177.
[22] N. Pereira, J.F. Al-Sharab, F. Cosandey, F. Badway, G.G. Amatucci, J. Electrochem. Soc. 155 (2008) A831–A838.
[23] N.M. Hagh, F. Cosandey, S. Rangan, R. Bartynski, G.G. Amatucci, J. Electrochem. Soc. 157 (2010) A305–A319.
[24] D.H. Cho, C.H. Jo, W. Cho, Y.J. Kim, H. Yashiro, Y.K. Sun, S.T. Myung, J. Electrochem. Soc. 161 (2014) A920–A926.
[25] J. Li, H.S. Liu, J. Xia, A.R. Cameron, M.Y. Nie, G.A. Botton, J.R. Dahn, J. Electrochem. Soc. 164 (2017) A655–A665.
[26] Y.M. Lee, K.M. Nam, E.H. Hwang, Y.G. Kwon, D.H. Kang, S.S. Kim, S.W. Song, J. Phys. Chem. C 118 (2014) 10631–10639.
[27] P. Ross, G. Somorjai, K. Komvopoulos, J. Phys. Chem. C (2017) 121.
[28] X.L. Liao, X.W. Zheng, J.W. Chen, Z.Y. Huang, M.Q. Xu, L.D. Xing, Y.H. Liao, Q. L. Lu, X.F. Li, W.S. Li, Electrochim. Acta 212 (2016) 352–359.
[29] H. Kuriyama, H. Saruwatari, H. Satake, A. Shima, F. Uesugi, H. Tanaka, T. Ushirogouchi, J. Power Sources 275 (2015) 99–105.
[30] M. Gaberscek, J. Moskon, B. Erjavec, R. Dominko, J. Jamnik, Electrochem. Solid St. 11 (2008) A170–A174.
[31] K.J. Nelson, D.W. Abarbanel, J. Xia, Z.H. Lu, J.R. Dahn, J. Electrochem. Soc. 163 (2016) A272–A280.
[32] D.W. Abarbanel, K.J. Nelson, J.R. Dahn, J. Electrochem. Soc. 163 (2016) A522–A529.
[33] J.M. Atebamba, J. Moskon, S. Pejovnik, M. Gaberscek, J. Electrochem. Soc. 157 (2010) A1218–A1228.
[34] M. Kerlau, M. Marcinek, V. Srinivasan, R.M. Kostecki, Electrochim. Acta 52 (2007) 5422–5429.
[35] G. Liu, H. Zheng, A.S. Simens, A.M. Minor, X. Song, V.S. Battaglia, J. Electrochem. Soc. 154 (2007) A1129–A1134.
[36] G. Liu, H. Zheng, S. Kim, Y. Deng, A.M. Minor, X. Song, V.S. Battaglia, J. Electrochem. Soc. 155 (2008) A887–A892.
[37] X.L. Li, F.Y. Kang, X.D. Bai, W. Shen, Electrochem. Commun. 9 (2007) 663–666.
[38] S. Watanabe, M. Kinoshita, T. Hosokawa, K. Morigaki, K. Nakura, J. Power Sources 260 (2014) 50–56.
[39] R. Petibon, L. Madec, D.W. Abarbanel, J.R. Dahn, J. Power Sources 300 (2015) 419–429.